Sensors and Materials, Vol. 37, No. 10 (2025) 4365–4381
MYU Tokyo

S & M 4187

Development of an Electrochemical Sensor with Nanozyme-modified Electrodes for Noninvasive Cortisol Analysis during Physical Activity

Chenglong Yan[1*] and Yuhong Ren[2]

[1]Wuhan Huaxia University of Technology, Hubei Wuhan 430223, China
[2]Hubei Institute of Sports Science, Wuhan Hubei 430205, China

(Received July 15, 2025; accepted August 27, 2025)

Keywords: cortisol monitoring, electrochemical aptasensor, gold nanozymes, sweat-based biosensing, screen-printed carbon electrodes

In this paper, we present details of the development of a disposable, noninvasive electrochemical aptasensor for the real-time monitoring of cortisol in human sweat. The sensor is fabricated on a flexible screen-printed carbon electrode (SPCE) modified with a novel conjugate of a cortisol-specific DNA aptamer and gold nanozymes (Au-NZs; gold nanoparticles that display enzyme-mimetic catalytic activity). This synergistic design leverages the aptamer's specificity and the peroxidase-like/oxidase-like activity reported for Au nanozymes, providing a stable, enzyme-free catalytic interface that supports robust electrochemical transduction and, where applicable, catalytic amplification. Electrochemical characterization using cyclic voltammetry (CV), electrochemical impedance spectroscopy (EIS), and differential pulse voltammetry (DPV) demonstrated superior conductivity and a clear detection mechanism based on cortisol binding. The sensor exhibited excellent analytical performance with a clinically relevant linear detection range of 5.0 to 150.0 ng/mL, a low limit of detection of 1.5 ng/mL, and high selectivity against physiological interferents. The sensor's practical utility was validated through the dynamic tracking of cortisol fluctuations in human sweat during physical exercise, showing an excellent correlation (r = 0.989) with the gold-standard ELISA method. This nanozyme-based platform represents a significant advancement toward accessible, point-of-care stress monitoring for applications in personalized medicine, sports science, and occupational health.

1. Introduction

Cortisol, the principal human glucocorticoid, is a definitive biomarker of physiological and psychological stress.(1) Its secretion is tightly regulated by the hypothalamic-pituitary-adrenal (HPA) axis(2) and follows a distinct circadian rhythm, characterized by a peak concentration shortly after awakening (cortisol awakening response)(3) and a gradual decline to a nadir around midnight.(4) This diurnal pattern is fundamental for maintaining homeostasis, and disruptions to

*Corresponding author: e-mail: yanlong0516@126.com
https://doi.org/10.18494/SAM5845

ISSN 0914-4935

this rhythm, such as a flattened diurnal cortisol slope, are recognized as a key indicator of HPA axis dysregulation.[5] Such dysregulation is clinically associated with a wide spectrum of adverse health outcomes, including major depressive disorder (MDD), chronic fatigue, obesity, and an increased risk for cardiovascular disease.[6] Consequently, the ability to accurately monitor cortisol dynamics provides a critical window into an individual's neuroendocrine function and overall health status.[7] The relationship between physical activity and cortisol secretion is complex and highlights the need for advanced monitoring technologies.[8] While regular physical activity in healthy individuals is generally associated with a more robust, steeper diurnal cortisol slope, suggesting improved HPA axis regulation,[9] the acute response to exercise can elicit a transient increase in cortisol level.[10] The cross-stressor-adaptation (CSA) hypothesis posits that repeated exposure to the physiological stress of exercise can attenuate the HPA axis response to subsequent psychosocial stressors. However, this adaptive response can differ significantly in clinical populations; for instance, individuals with MDD may exhibit a blunted or entirely unresponsive cortisol reaction to stressors.[11] This variability underscores a critical limitation of conventional monitoring methods. Single-point or infrequent measurements fail to capture the complete dynamic profile of the cortisol response—including the magnitude, peak time, and recovery rate—which is essential for distinguishing between a healthy, adaptive HPA axis and a dysregulated one. This analytical gap necessitates the development of sensors capable of continuous, real-time tracking to provide a richer, more personalized dataset.[12]

Current gold-standard methods for cortisol quantification, such as enzyme-linked immunosorbent assay (ELISA) and high-performance liquid chromatography (HPLC), are ill-suited for real-time, point-of-care (PoC) applications. These laboratory-based techniques typically rely on invasive blood sampling, require extensive sample preparation, and are characterized by long turnaround times, high costs, and susceptibility to analytical interferences, such as matrix effects and systematic bias.[13] Sweat has emerged as an ideal alternative biofluid for noninvasive monitoring.[14] It is readily accessible, and the concentration of free, biologically active cortisol in sweat shows a strong correlation with circulating levels in blood and saliva,[15] making it a physiologically relevant matrix for dynamic stress assessment.[16]

Electrochemical biosensors offer a promising technological platform to harness the diagnostic potential of sweat.[17] These devices are inherently portable, highly sensitive, selective, and cost-effective, making them amenable to mass production and integration into wearable formats for continuous monitoring.[18] The performance of these sensors is largely dictated by the biorecognition element immobilized on the electrode surface, which typically consists of antibodies, aptamers, or molecularly imprinted polymers (MIPs).[19] While antibodies are widely used, they often suffer from limited stability in nonideal environmental conditions, a significant drawback for field-deployable devices. In contrast, synthetic DNA or RNA aptamers offer superior thermal and chemical stabilities, reproducible chemical synthesis, and a lack of immunogenicity, positioning them as a more robust choice for wearable sensor development. Notably, Sharma *et al.*[20] reported an electrochemical cortisol aptasensor in which a truncated 14-mer aptamer was immobilized on gold-nanoparticle-modified screen-printed electrodes for saliva analysis, achieving a dynamic range of 0.1 pg mL^{-1}–100 ng mL^{-1} and limits of detection of 0.25 pg mL^{-1} (buffer) and 0.28 pg mL^{-1} (artificial saliva). In contrast, our present work targets

sweat during physical activity using a gold nanozyme–aptamer interface on screen-printed carbon electrodes, with a linear range of 5.0–150.0 ng mL^{-1}, tailored to the typical sweat cortisol window (8–142 ng mL^{-1}) and validated against ELISA in real exercise with r = 0.989. This juxtaposition underscores matrix-specific design choices (saliva vs sweat), distinct transducer chemistries (AuNP immobilization vs catalytically active Au-nanozyme interface), and different validation emphases (static saliva vs dynamic sweat during exercise).

In this work, we introduce a novel electrochemical sensing platform that capitalizes on a synergistic combination of a highly stable DNA aptamer for specific cortisol recognition and catalytically active gold nanozymes (Au-NZs) for signal transduction. Unlike nanomaterials used solely to increase the interfacial area, Au-NZs act as artificial enzyme mimics ('nanozymes')—gold nanoparticles with intrinsic peroxidase-like and, in certain systems, oxidase-like activity—providing a stable, enzyme-free catalytic center compatible with electrochemical signal generation and amplification. This definition follows the nanozyme literature and recent reports on gold-based nanozymes used in electroanalytical devices.[21,22] This dual-functionality design circumvents the stability issues of natural enzymes (e.g., horseradish peroxidase) often used in electrochemical immunoassays, resulting in a more robust sensor. The objective of this study is therefore to design, fabricate, and comprehensively validate a disposable electrochemical aptasensor, based on a screen-printed electrode modified with this Au-NZ-aptamer conjugate, for the rapid and noninvasive quantification of cortisol dynamics in human sweat collected during physical activity.

2. Materials and Methods

2.1 Chemicals and reagents

Cortisol (hydrocortisone, CAS No. 50-23-7), gold(III) chloride trihydrate ($HAuCl_4{\cdot}3H_2O$, CAS No. 16961-25-4), trisodium citrate dihydrate (CAS No. 6132-04-3), potassium hexacyanoferrate(II) trihydrate ($K_4[Fe(CN)_6]{\cdot}3H_2O$, CAS No. 14459-95-1), potassium hexacyanoferrate(III) ($K_3[Fe(CN)_6]$, CAS No. 13746-66-2), potassium phosphate monobasic (KH_2PO_4), and potassium phosphate dibasic (K_2HPO_4) were purchased from Sigma-Aldrich (St. Louis, MO, USA). The 5'-thiolated DNA aptamer specific for cortisol (sequence: 5'-SH-$(CH_2)_6$-ACA CTA GGC TTA CGG TAC GGT AGG-3') was custom-synthesized by Integrated DNA Technologies (Coralville, IA, USA). For the context and benchmarking of cortisol aptamer performance, prior literature reports include the capture-SELEX cortisol aptamer '15-1' with solution K_d values of 6.9 ± 2.8 μM (equilibrium dialysis) and 16.1 ± 0.6 μM (microscale thermophoresis) and limited utility upon truncation; the independently selected aptamer 'CSS.1' with $K_d \approx$ 245 nM by ITC and confirmed selectivity against deoxycholic acid, 17β-estradiol, thymidine, and dopamine in buffer; and a more recent cortisol aptamer deployed on In_2O_3 FETs with $K_d \approx$ 500 nM in solution and ~30 pM on-device, showing discrimination over corticosterone, testosterone, and aldosterone.[23,24] Potential interfering agents, including cortisone, glucose, lactic acid, ascorbic acid, and uric acid, were also obtained from Sigma-Aldrich. All reagents were of analytical grade and used without further purification.

2.2 Synthesis of Au-NZs

Spherical Au-NZs were synthesized using a modified Turkevich citrate reduction method.[25] Briefly, 50 mL of 0.01% (w/v) $HAuCl_4$ solution was heated to a vigorous boil in a round-bottom flask under constant stirring. Subsequently, 1.5 mL of 1% (w/v) trisodium citrate solution was rapidly added to the boiling solution. The color of the solution changed from pale yellow to gray, then to purple, and finally to a stable ruby-red within minutes, indicating the formation of Au-NZs. The solution was kept boiling and stirred for an additional 15 min to ensure the reaction completion. After cooling to room temperature, the resulting colloidal Au-NZ solution was stored at 4 °C until use. This method consistently produced nanoparticles with an average diameter of approximately 40–50 nm.

2.3 Functionalization of Au-NZs with cortisol aptamer

The Au-NZ-Aptamer conjugate was prepared by incubating the synthesized Au-NZs with the thiolated cortisol aptamer. 2 μM 5'-thiol-modified DNA aptamer solution was added to the colloidal Au-NZ solution and gently agitated at room temperature for 12 h. This process facilitates the formation of a stable, self-assembled monolayer of aptamers on the gold surface via dative Au-S bonds.[26] To remove unbound aptamers, the conjugate solution was purified through three cycles of centrifugation at 12000 rpm for 20 min, followed by the removal of the supernatant and the resuspension of the pellet in 10 mM phosphate-buffered saline (PBS, pH 7.4). The final purified Au-NZ-Aptamer conjugate was stored at 4 °C.

2.4 Fabrication of nanozyme-modified screen-printed electrode (Au-NZ-Apt/SPE)

Commercially available flexible screen-printed carbon electrodes (SPCEs, DropSens, DRP-110) fabricated on a polyethylene terephthalate (PET) substrate were used as the sensor platform. Each SPE consists of a carbon working electrode (WE, 4 mm diameter), a carbon counter electrode (CE), and a Ag/AgCl pseudo-reference electrode (RE). The fabrication of the final sensor involved a two-step modification process. First, the SPEs were electrochemically cleaned and activated by performing 10 cyclic voltammetry (CV) scans from −0.2 to +1.3 V at 100 mV/s in 0.1 M H_2SO_4, followed by thorough rinsing with DI water. Second, the Au-NZ-aptamer conjugate was immobilized onto the WE surface by drop-casting 10 μL of the purified conjugate solution. The modified electrode was then allowed to dry slowly in a humidified chamber at room temperature for 2 h to ensure the formation of a uniform and stable sensing layer.[27] The resulting sensor is denoted as Au-NZ-Apt/SPE.

2.5 Electrochemical measurements

All electrochemical experiments were conducted in a Faraday cage at room temperature (25 ± 1 °C). A three-electrode setup was used with the modified SPE. The electrolyte for all measurements was 10 mM PBS (pH 7.4) containing 5 mM $[Fe(CN)_6]^{3-/4-}$ as a redox probe. CV

was performed by scanning at a rate of 50 mV/s. Electrochemical impedance spectroscopy (EIS) was conducted over a frequency range from 100 kHz to 0.1 Hz, with a sinusoidal AC voltage of 10 mV amplitude superimposed on the formal potential of the redox couple. Differential pulse voltammetry (DPV) was used for quantitative cortisol detection, with a pulse amplitude of 50 mV, a pulse width of 50 ms, and a step potential of 5 mV. For detection, the Au-NZ-Apt/SPE was incubated in standard cortisol solutions or sweat samples for an optimized period of 20 min, followed by a brief rinse with PBS to remove nonspecifically bound molecules before the DPV measurement.

2.6 Human subject protocol and real sample analysis

Sweat samples were collected from 10 healthy volunteers (5 male, 5 female, age 25–35 years) following an IRB-approved protocol. Each subject first rested for 5 min, after which they performed 20 min of cycling on a stationary ergometer at an intensity corresponding to 70% of their age-predicted maximum heart rate. Sweat was collected noninvasively from the subject's back using a sterile Macroduct® sweat collection system at four time points: 0 min (baseline, pre-exercise), 10 min (during exercise), 20 min (end of exercise), and 40 min (20 min post-exercise). For the recovery study, sweat samples from all volunteers were pooled. The pooled sample was divided into four aliquots: one was left unspiked, while the other three were spiked with cortisol to achieve final concentrations of 10, 50, and 100 ng/mL. These samples were analyzed using the developed sensor to assess matrix effects and determine the recovery percentage. For validation, all collected human sweat samples were also analyzed using a commercial salivary cortisol enzyme-linked immunosorbent assay (ELISA) kit (Salimetrics LLC, State College, PA, USA) according to the manufacturer's instructions.

2.7 Catalytic activity assays for Au-NZs

Au-NZ peroxidase-like activity was assessed by monitoring the oxidation of 3,3′,5,5′-tetramethylbenzidine (TMB, 0.5 mM) in acetate buffer (pH 4.0) containing H_2O_2 (0.1–5 mM) at 652 nm. Control reactions lacking Au-NZs or H_2O_2 were run in parallel. Apparent Michaelis–Menten parameters (K_M, V_{max}) were estimated from initial rates versus substrate concentration; assay conditions follow established Au nanozyme protocols. In a complementary electrochemical assay, chronoamperometry (0.0 V to −0.3 V vs Ag/AgCl) on the bare and Au-NZ-modified SPEs quantified catalytic reduction currents for stepwise H_2O_2 additions in PBS (pH 7.4).

3. Results and Discussion

3.1 Characterization of the Au-NZ-aptamer conjugate

The successful synthesis and functionalization of the Au-NZ-aptamer conjugate, the core component of the sensor, were confirmed through extensive material characterization. Figure 1

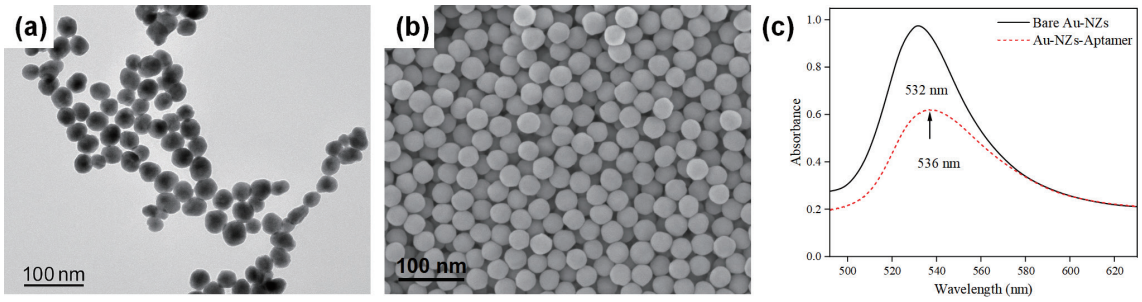

Fig. 1. (Color online) Morphological and optical characterization of Au-NZs and Au-NZ-aptamer conjugate. (a) TEM image of synthesized Au-NZs. (b) SEM image of Au-NZs. (c) UV-Vis absorption spectra of bare Au-NZs and Au-NZ-aptamer conjugate, showing a characteristic redshift upon aptamer binding.

presents the morphological and optical properties of the nanomaterials. TEM imaging [Fig. 1(a)] and SEM imaging [Fig. 1(b)] revealed the formation of highly monodisperse, spherical gold nanoparticles with a narrow size distribution and an average diameter of 45±5 nm. The nanoparticles exhibited no signs of aggregation, indicating good colloidal stability provided by the citrate capping layer.[28] The optical properties were assessed by UV–Vis spectroscopy [Fig. 1(c)]. The bare Au-NZs displayed a sharp and symmetric localized surface plasmon resonance (LSPR) peak centered at 532 nm, which is characteristic of spherical gold nanoparticles of this size.[25] Upon functionalization with the thiolated aptamer, this LSPR peak underwent a bathochromic shift from 532 to 536 nm. This shift is attributed to the change in the local dielectric environment surrounding the nanoparticles upon the binding of the DNA aptamer to the gold surface, providing the first piece of evidence for successful surface conjugation.

The structural and crystalline nature of the synthesized nanozymes was investigated by XRD. The results are shown in Fig. 2(a). The XRD pattern exhibits four distinct diffraction peaks at 2θ values of 38.2, 44.4, 64.6, and 77.5°. These peaks correspond to the (111), (200), (220), and (311) crystallographic planes of the face-centered cubic (fcc) lattice of metallic gold, respectively (JCPDS Card No. 04-0784).[29] The sharpness and intensity of the peaks, particularly the dominant (111) peak, confirm the high degree of crystallinity of the synthesized Au-NZs. No peaks corresponding to impurities were observed, indicating the purity of the material. The crystalline nature is crucial for the stable electronic and catalytic properties of the nanozymes.

FTIR spectroscopy was employed to provide direct chemical evidence of aptamer immobilization on the Au-NZ surface [Fig. 2(b)]. The spectrum of the bare Au-NZs shows only minor peaks associated with residual citrate. The spectrum of the free aptamer displays characteristic peaks corresponding to the DNA structure, including a strong band at ~1080 cm^{-1} from the symmetric stretching of the phosphate (PO_2^-) backbone and multiple peaks between 1400 and 1700 cm^{-1} from the vibrations of the purine and pyrimidine bases. In the spectrum of the Au-NZ-aptamer conjugate, these characteristic DNA peaks, notably the prominent phosphate backbone peak at a slightly shifted position of ~1085 cm^{-1} and the base-related vibrations, are clearly visible.[30] The presence of these peaks confirms the successful attachment of the aptamer molecules to the nanozyme surface.

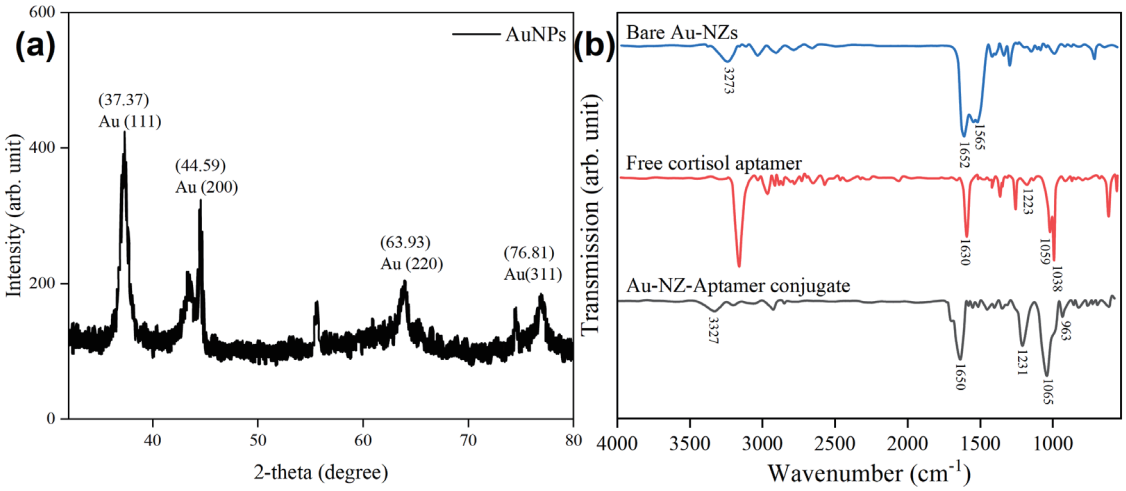

Fig. 2. (Color online) (a) XRD pattern of synthesized Au-NZs. The diffraction peaks are indexed to the (111), (200), (220), and (311) planes of the fcc structure of metallic gold, confirming the high crystallinity of the nanoparticles. (b) FTIR spectra of bare Au-NZs, free cortisol aptamer, and Au-NZ-aptamer conjugate.

Further confirmation of the surface composition and the chemical state of gold was obtained via XPS analysis (Fig. 3). The survey scan [Fig. 3(a)] confirmed the presence of Au, C, N, O, and P in the Au-NZ-aptamer conjugate. The high-resolution Au 4f spectrum [Fig. 3(b)] shows two sharp peaks at binding energies of 84.0 and 87.7 eV, corresponding to the Au $4f_{7/2}$ and Au $4f_{5/2}$ spin-orbit doublets, respectively. This confirms that the gold in the nanozymes exists in its metallic, zero-valent state (Au^0), which is essential for its catalytic activity and stability.[31] The high-resolution spectra for N 1s [Fig. 3(c)] and P 2p [Fig. 3(d)] show distinct peaks that are absent in the bare nanoparticles, providing definitive evidence of the presence of the nitrogenous bases and phosphate backbone of the DNA aptamer on the nanozyme surface.

3.2 Electrochemical characterization of the sensor assembly

The step-by-step fabrication of the sensor on the SPE platform was monitored using both SEM and electrochemical techniques. The SEM imaging of the bare carbon working electrode [Fig. 4(a)] shows a relatively flat surface of carbon ink. In contrast, the image of the Au-NZ-Apt/SPE [Fig. 4(b)] reveals a uniform and dense layer of the nanozyme conjugates distributed across the electrode surface, confirming a successful and well-controlled immobilization process.[32] This high-density coating is critical for achieving a sensitive and reproducible sensor response.

The electrochemical properties of the electrode at each modification stage were investigated using CV and EIS in the presence of the $[Fe(CN)_6]^{3-/4-}$ redox probe (Fig. 5). The bare SPE exhibited slow electron transfer kinetics characterized by a large peak potential separation (ΔEp) in the CV and a large semicircle in the Nyquist plot, corresponding to a high charge-transfer resistance (*Rct*). Upon modification with the Au-NZ-aptamer conjugate, a marked improvement in electrochemical performance was observed. The redox peak currents in the CV increased significantly and ΔEp decreased, approaching the ideal value for a reversible one-electron process. Concurrently, the diameter of the Nyquist semicircle in the EIS plot decreased

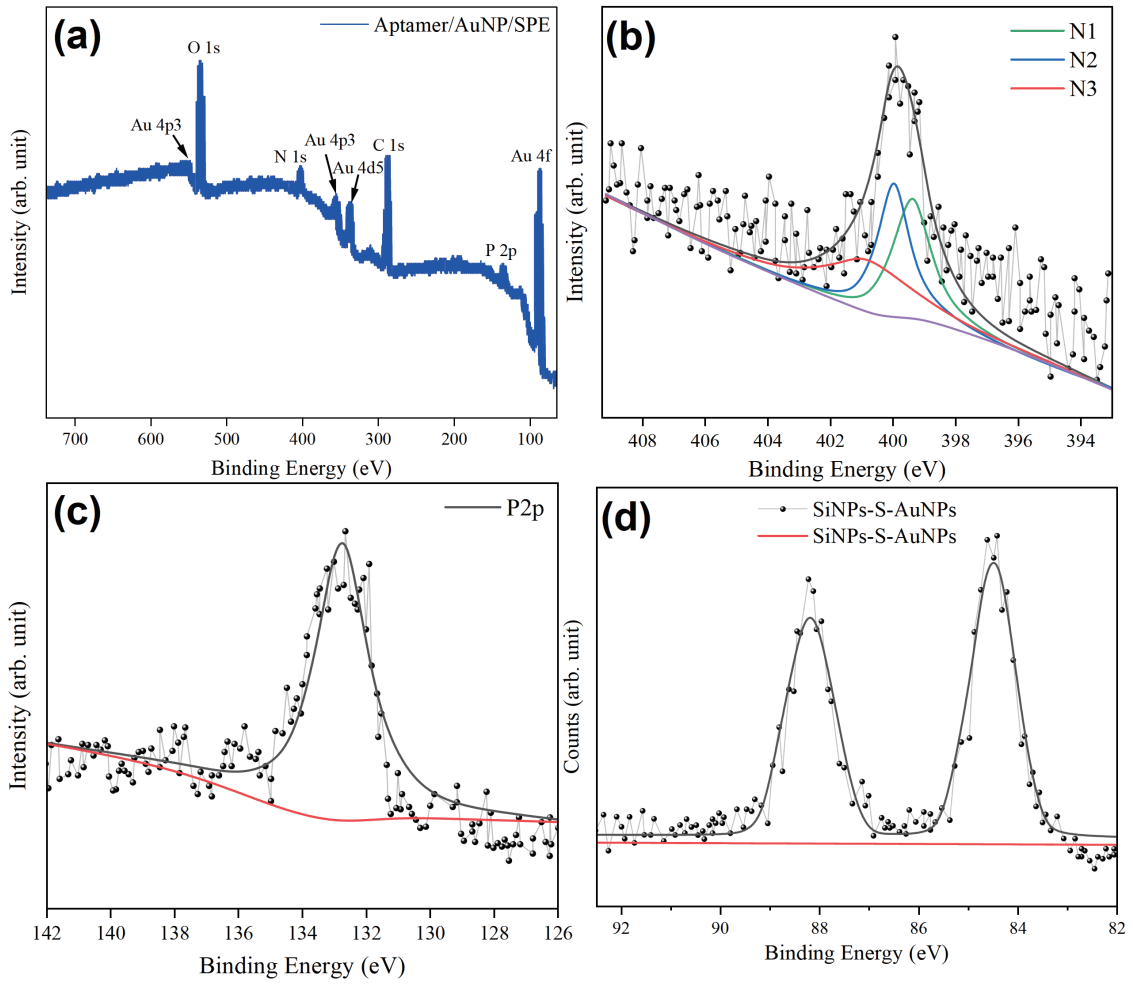

Fig. 3. (Color online) High-resolution XPS spectra of Au-NZ-aptamer conjugate. (a) Full survey scan. (b) Au 4f spectrum confirming the metallic Au(0) state. (c) N 1s spectrum and (d) P 2p spectrum confirming the presence of the DNA aptamer on the surface.

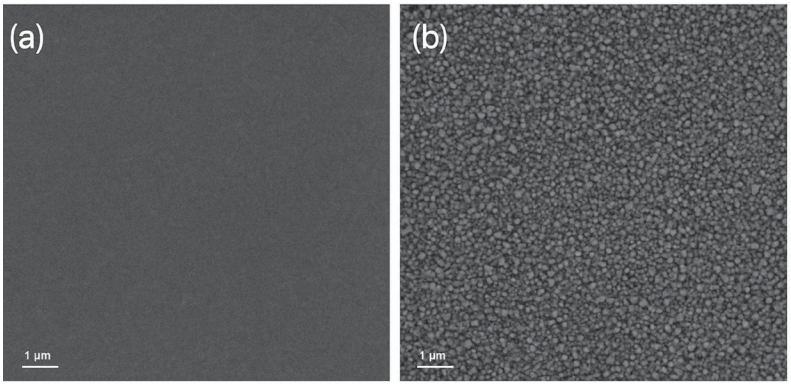

Fig. 4. SEM images of the electrode surface. (a) Bare SPE. (b) SPE modified with the Au-NZ-aptamer conjugate, showing a dense and uniform coating.

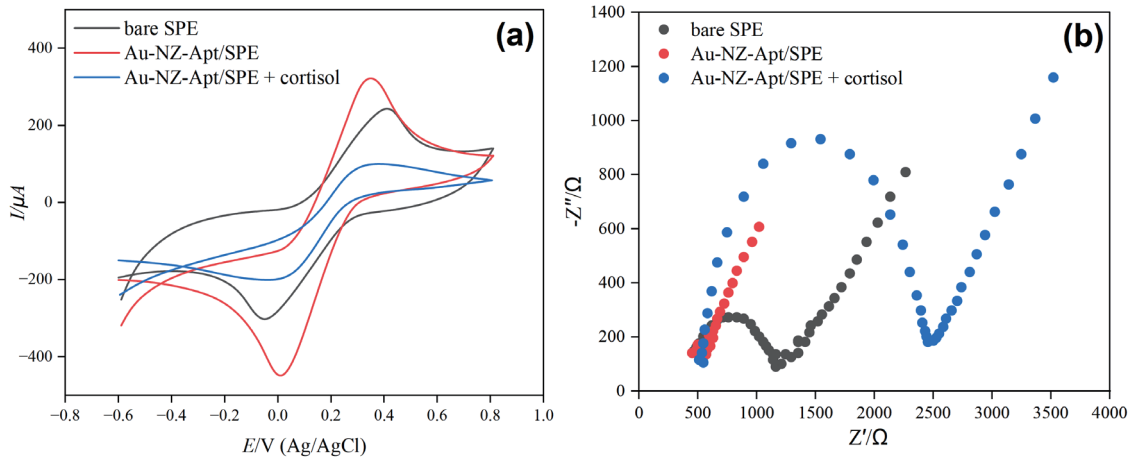

Fig. 5. (Color online) Stepwise electrochemical characterization of the sensor fabrication. (a) Cyclic voltammograms and (b) EIS Nyquist plots of bare SPE, Au-NZ-Apt/SPE, and Au-NZ-Apt/SPE after binding with 100 ng/mL cortisol in 10 mM PBS (pH 7.4) containing 5 mM $[Fe(CN)_6]^{3-/4-}$.

substantially. This indicates a significant acceleration of the electron transfer kinetics, which is attributed to the excellent conductivity and high surface area of the Au-NZ layer.[33] After incubation with 100 ng/mL cortisol, the aptamers on the surface undergo a conformational change to bind the cortisol molecules. This binding event forms an insulating layer on the electrode surface, which hinders the access of the redox probe to the electrode. Consequently, the redox peak currents in the CV decreased and the *Rct* in the EIS plot increased markedly. This clear and predictable change in electrochemical behavior validates the sensing mechanism of the platform.[34] In addition, the Au-NZ coating furnishes an enzyme-free catalytic interface; its peroxidase-like activity was verified by a TMB/H_2O_2 assay and an electrochemical H_2O_2 test (Methods 2.7), consistent with the gold nanozyme behavior reported in the literature.

To quantify these observations, the EIS data were fitted to a Randles equivalent circuit model, and the resulting parameters are summarized in Table 1. The model consists of the solution resistance (*Rs*), *Rct*, and a constant phase element (CPE) representing the double-layer capacitance. The fitting results provide a quantitative basis for the changes observed in Fig. 5. The *Rct* value for the bare SPE was 852 Ω. After modification with the Au-NZ-Apt conjugate, *Rct* decreased markedly to 95 Ω, a nearly 9-fold reduction that numerically confirms the superior conductivity of the nanozyme-modified surface. Following incubation with 100 ng/mL cortisol, *Rct* increased to 456 Ω, confirming the formation of an insulating layer owing to aptamer-cortisol binding. The solution resistance (*Rs*) remained relatively constant throughout the modification process, as expected. This rigorous quantitative analysis validates both the enhanced performance of the sensor platform and the proposed detection mechanism.[33]

3.3 Optimization and analytical performance

To ensure optimal sensor performance, key experimental parameters were optimized. The effect of pH on the sensor's response to 50 ng/mL cortisol was investigated over a range from 6.0 to 8.5 [Fig. 6(a)]. The DPV signal change was maximal at pH 7.4, which corresponds to

Table 1
EIS fitting parameters for the modified electrode at each fabrication step.

Modification step	*Rs* (Ω)	*Rct* (Ω)	CPE-T (μF·s^{n-1})	CPE-*n*
Bare SPE	55.2	852	15.6	0.85
Au-NZ-Apt/SPE	54.8	95	38.2	0.92
+ 100 ng/mL Cortisol	56.1	456	25.4	0.88

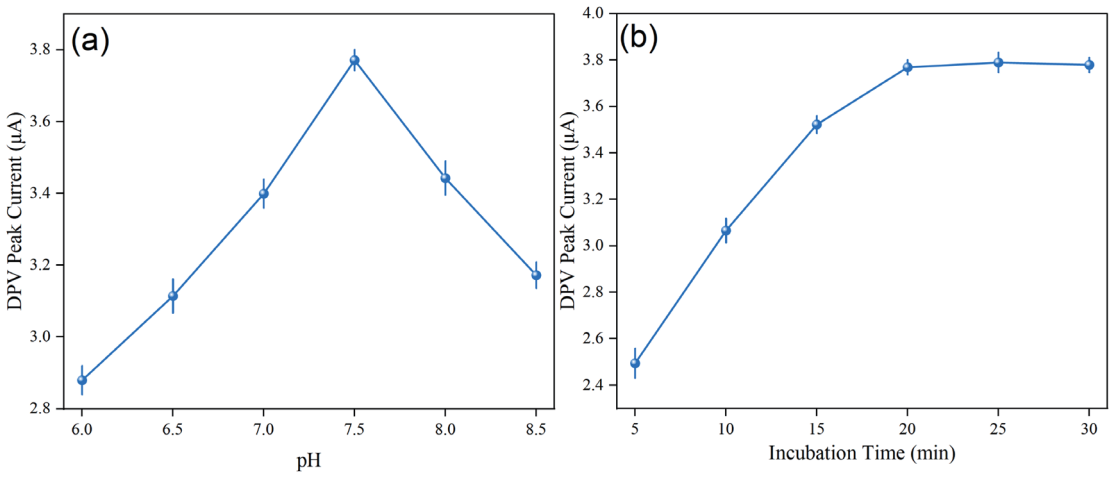

Fig. 6. (Color online) Optimization of assay parameters. (a) Effect of pH on the DPV current response to 50 ng/mL cortisol. (b) Effect of incubation time on the DPV current response to 50 ng/mL cortisol. Optimal conditions were determined to be pH 7.4 and an incubation time of 20 min.

physiological pH and is ideal for biological sample analysis. Therefore, pH 7.4 was selected for all subsequent experiments. The incubation time required for the binding reaction between the aptamer and the cortisol to reach equilibrium was also optimized [Fig. 6(b)]. The DPV signal change increased with incubation time and reached a plateau after approximately 20 min, indicating that the binding sites were saturated. Thus, an incubation time of 20 min was adopted to ensure a stable and maximal response.[26] While the main transduction in this work leverages the aptamer-mediated modulation of $[Fe(CN)_6]^{3-/4-}$ electron transfer, the Au-NZ layer constitutes a catalytically active (peroxidase-like/oxidase-like) surface. Such activity is widely exploited to amplify signals in electrochemical biosensors, including cortisol assays employing gold-based nanozymes, and positions our platform for enzyme-free catalytic amplification in future wearable formats.

Under these optimized conditions, the analytical performance of the Au-NZ-Apt/SPE for cortisol detection was evaluated by DPV. Figure 7(a) shows the DPV responses of the sensor after incubation with different concentrations of cortisol ranging from 1 to 200 ng/mL. A clear, concentration-dependent decrease in the peak current of the $[Fe(CN)_6]^{3-/4-}$ redox probe was observed. This demonstrates that as more cortisol molecules bind to the aptamers, the electron transfer to the electrode surface is increasingly blocked, resulting in a lower electrochemical signal.

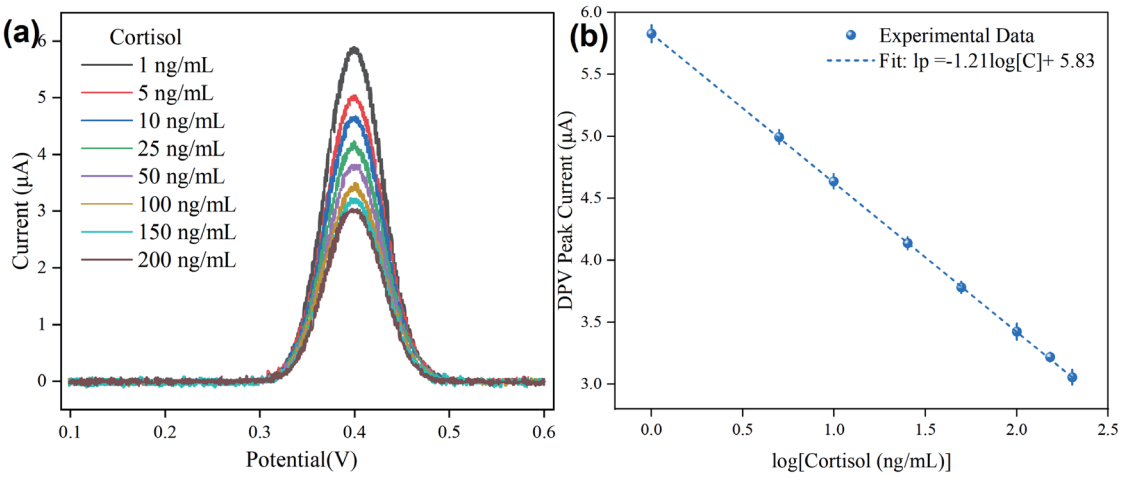

Fig. 7. (Color online) (a) DPV response curves of Au-NZ-Apt/SPE for increasing concentrations of cortisol (from top to bottom: 1, 5, 10, 25, 50, 100, 150, and 200 ng/mL) in PBS (pH 7.4). (b) Calibration curve for Au-NZ-Apt/SPE. The plot shows the DPV peak current as a function of the logarithm of cortisol concentration. The linear range is 5.0–150.0 ng/mL with R^2 of 0.995.

The calibration curve for the sensor was constructed by plotting the DPV peak current against the logarithm of the cortisol concentration [Fig. 7(b)]. The sensor exhibited a well-defined linear response over the concentration range of 5.0 to 150.0 ng/mL. This range is highly relevant for practical applications as it covers the typical physiological concentrations of cortisol found in human sweat (8–142 ng/mL).[35] The linear regression equation was determined to be Ip (μA) = −1.21log[cortisol (ng/mL)] + 5.83, with an excellent correlation coefficient (R^2) of 0.995. The limit of detection (LOD) was calculated to be 1.5 ng/mL using the formula $3\sigma/S$, where σ is the standard deviation of the blank signal and S is the sensitivity (slope of the calibration curve). This low LOD ensures that the sensor can reliably detect even baseline levels of cortisol.[36]

The performance of the developed sensor was benchmarked against other recently reported electrochemical cortisol sensors, as summarized in Table 2. While some immunosensors report lower LODs, these often fall outside the physiologically relevant range for sweat analysis.[37] The Au-NZ-Apt/SPE developed in this work provides a combination of a low, clinically relevant LOD and a practical linear range. In particular, Sharma *et al.*[20] fabricated a saliva aptasensor by immobilizing a truncated 14-mer cortisol aptamer on AuNP-modified SPEs and reported a dynamic range of 0.1 pg/mL–100 ng/mL with LODs of 0.25 pg/mL (buffer) and 0.28 pg/mL (artificial saliva). Our Au-nanozyme–aptamer SPCE sensor exhibits a linear range of 5.0–150.0 ng/mL with an LOD of 1.5 ng/mL, closely matching the physiological concentration window in sweat (8–142 ng/mL) and thereby prioritizing on-body relevance over ultralow LODs optimized for saliva. Beyond analytical figures, our study advances real-world validation by tracking exercise-induced cortisol dynamics in sweat and demonstrating near-identity with ELISA (r = 0.989), whereas Sharma *et al.* focused primarily on artificial saliva and spiked saliva analyses. Mechanistically, their AuNPs principally serve as a high-surface-area immobilization scaffold, while our Au nanozymes additionally endow enzyme-mimetic catalytic activity, providing a robust, enzyme-free interface suitable for future catalytic amplification in wearables.

Table 2
Analytical performance characteristics of the developed sensor and other reported electrochemical cortisol sensors.

Sensor Platform	Bioreceptor	Detection Range	LOD	Reference
Au-plated Textile	MIP	10–66 ng/mL	2.0 ng/mL	(38)
Graphene/AuNP	Aptamer	1 pM–1 μM	0.68 nM	(26)
AuNP/MoS_2/AuNP	Antibody	0.5–200 nM	0.11 nM	(39)
SnS_2/NiCo MOF/AuNP	Antibody	100 fg/mL–100 ng/mL	29 fg/mL	(40)
AuSPE	Aptamer	0.1 pg/mL–100 ng/mL	0.28 pg/mL	(20)
Au-NZ-Apt/SPE	Aptamer	5.0–150.0 ng/mL	1.5 ng/mL	This work

More importantly, its reliance on a highly stable nanozyme-aptamer system offers significant advantages in terms of robustness and shelf-life compared with sensors based on less stable biological components, such as antibodies or natural enzymes, making it particularly well suited to point-of-care and wearable applications.

3.4 Selectivity, reproducibility, and stability studies

For a biosensor to be practical for real-world sample analysis, it must exhibit high selectivity, reproducibility, and stability. The selectivity of the Au-NZ-Apt/SPE was evaluated by testing its response to cortisol in the presence of several potential interfering substances commonly found in sweat at high concentrations, including cortisone (a structurally similar steroid), glucose, lactic acid, and uric acid. In addition to our experimental selectivity data, prior cortisol-aptamer studies provide orthogonal evidence of chemical specificity against structurally related steroids. The CSS.1 aptamer exhibited binding to cortisol with $K_d \approx 245$ nM in ITC and showed no measurable binding to several non-targets (deoxycholic acid, 17β-estradiol, thymidine, and dopamine) under tested conditions. Separately, a recently reported cortisol aptamer used in a wearable FET platform demonstrated the selective recognition of cortisol over corticosterone, testosterone, and aldosterone in solution assays while achieving an on-device apparent K_d in the tens of picomolar range.(24) As shown in Fig. 8(a), the sensor's response to 25 ng/mL cortisol solution was significant, while its response to 100-fold higher concentrations of the interfering species was negligible (<5%). This demonstrates the high specificity of the aptamer for cortisol, a critical requirement for accurate analysis in a complex biological matrix.(41)

The reproducibility of the sensor was assessed by fabricating five independent Au-NZ-Apt/SPEs and measuring their responses to 50 ng/mL cortisol solution. The *RSD* of the measurements was calculated to be 4.2%, indicating excellent fabrication consistency and measurement reproducibility. The long-term stability of the sensor was also investigated by storing the modified electrodes at 4 °C for 30 days and periodically testing their response. The sensor retained more than 92% of its initial signal response after one month [Fig. 8(b)], highlighting the exceptional stability of the Au-NZ-aptamer conjugate compared with traditional enzyme- or antibody-based systems. This robustness is a key advantage for developing a practical, marketable device.

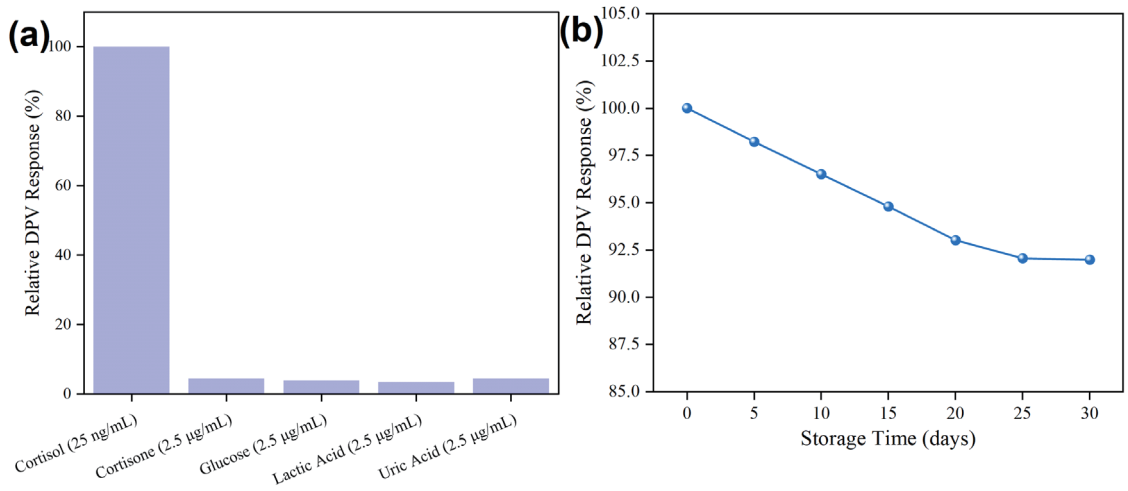

Fig. 8. (Color online) Sensor specificity and stability. (a) Selectivity of Au-NZ-Apt/SPE. The response to 25 ng/mL cortisol solution in the presence of 2.5 µg/mL cortisone, glucose, lactic acid, and uric acid. (b) Long-term stability of the sensor stored at 4 ℃ over 30 days.

3.5 Real-world application and validation

The ultimate test of a biosensor is its performance with real biological samples. To validate the practical applicability of the Au-NZ-Apt/SPE, a recovery study was performed using pooled human sweat. Known concentrations of cortisol were spiked into the sweat samples, and the recovery rate was calculated to assess the accuracy of the sensor in a complex matrix. As shown in Table 3, the sensor demonstrated excellent recovery rates ranging from 96.3 to 104.5% for all spiking concentrations. These results confirm that the complex components of human sweat do not significantly interfere with the sensor's accuracy, validating its suitability for direct sweat analysis.[42]

The sensor was then used to monitor the dynamic changes in sweat cortisol levels of a representative healthy volunteer during a controlled physical activity protocol. As depicted in Fig. 9, the sweat cortisol concentration was at a baseline level before exercise, increased significantly during the 20 min cycling session, peaked at the cessation of exercise, and then began to decline during the recovery period. This observed pattern aligns perfectly with the expected physiological response of the HPA axis to acute physical stress, demonstrating the sensor's capability to track dynamic hormonal fluctuations in real time.[43]

Finally, to establish the accuracy of the developed sensor, all 40 human sweat samples were analyzed using both the Au-NZ-Apt/SPE and a commercial ELISA kit, the current gold standard. A correlation plot of the results obtained by the two methods is shown in [Fig. 10(a)]. The data reveal a strong positive correlation with Pearson's correlation coefficient (r) of 0.989, indicating excellent agreement between the two methods. To further assess this agreement and check for systematic bias, a Bland–Altman analysis was performed [Fig. 10(b)]. The plot shows that 95% of the data points (38 out of 40) fall within the 95% limit of agreement (mean difference ± 1.96 SD), and the data points are randomly scattered around the mean difference line, which is close to zero. This confirms the absence of any significant systematic bias between the sensor and the

Table 3
Recovery of cortisol in spiked human sweat samples (n = 3).

Initial [Cortisol] (ng/mL)	Spiked [Cortisol] (ng/mL)	Measured [Cortisol] (ng/mL)	Recovery (%)	*RSD* (%)
14.5	10.0	24.8 ± 1.1	103.0	4.4
14.5	50.0	62.9 ± 2.5	98.8	4.0
14.5	100.0	110.8 ± 4.1	96.3	3.7

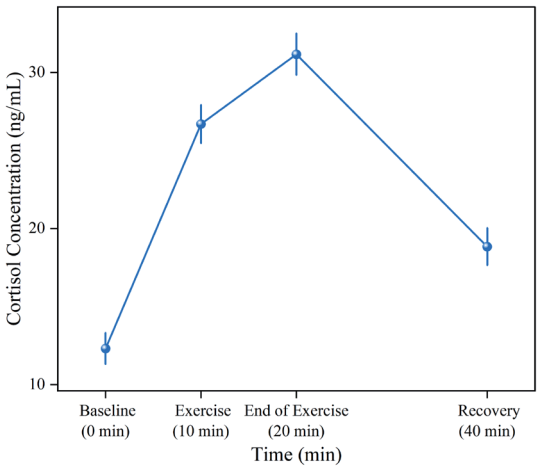

Fig. 9. (Color online) Dynamic monitoring of sweat cortisol from a representative subject during a physical exercise protocol. Cortisol levels were measured at baseline (0 min), during exercise (10 min), at the end of exercise (20 min), and during recovery (40 min).

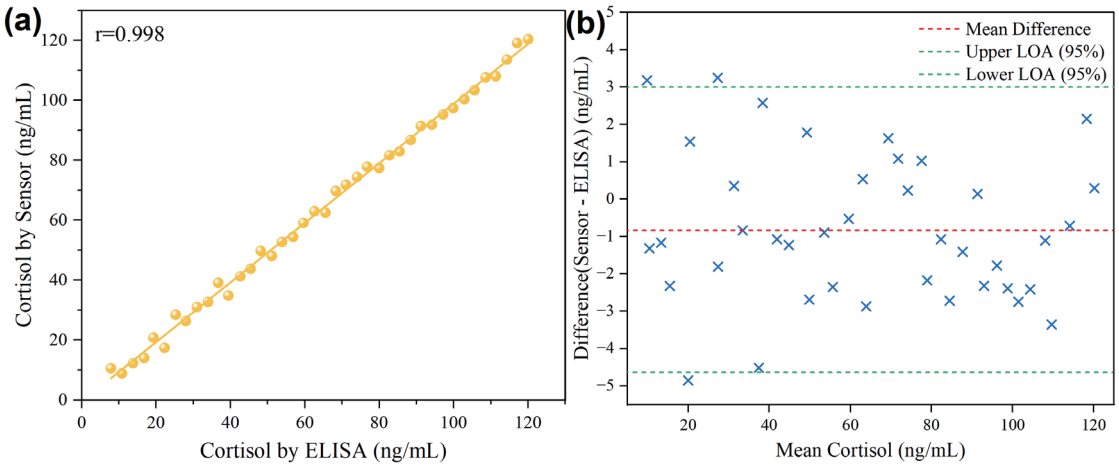

Fig. 10. (Color online) Validation of Au-NZ-Apt/SPE against the gold-standard ELISA method. (a) Correlation plot of cortisol concentrations in human sweat samples (n = 40) measured using the sensor and ELISA (r = 0.989). (b) Bland–Altman plot showing the agreement between the two methods.

ELISA method.[27] This comprehensive validation demonstrates that the developed low-cost, rapid, and noninvasive electrochemical sensor provides results that are statistically comparable to those obtained by the established, complex laboratory-based method.

4. Conclusions

In this research, a novel, disposable electrochemical aptasensor for the noninvasive analysis of cortisol in human sweat was successfully designed, fabricated, and comprehensively validated. The core innovation of this work lies in the development of a synergistic sensing platform that integrates the high specificity and stability of a DNA aptamer with the robust catalytic activity and conductivity of gold nanozymes. This Au-NZ-aptamer conjugate, immobilized on a low-cost screen-printed carbon electrode, overcomes the inherent stability limitations of conventional biosensors that rely on natural enzymes or antibodies, making it exceptionally well suited to point-of-care and wearable applications.

The developed sensor demonstrated excellent analytical performance, including a low limit of detection of 1.5 ng/mL and a linear detection range of 5.0–150.0 ng/mL, which is ideally matched to the physiological concentrations of cortisol in sweat. Furthermore, the sensor exhibited outstanding selectivity against common physiological interferents, high reproducibility ($RSD < 4.5\%$), and marked long-term stability, retaining more than 92% of its activity after 30 days of storage. The practical utility of the sensor was rigorously established through its successful application to real-world samples. It accurately quantified cortisol in spiked human sweat with recovery rates exceeding 96% and effectively tracked the dynamic physiological fluctuations of cortisol in response to physical exercise. Critically, the sensor's measurements showed a strong correlation ($r = 0.989$) and excellent agreement with the gold-standard ELISA method, confirming its accuracy and reliability.

In conclusion, this work presents a significant advancement in the field of electrochemical biosensing. By creating a robust, sensitive, and low-cost device, this research paves the way for accessible, real-time stress monitoring. The developed technology holds considerable promise for transformative applications in diverse fields, including personalized medicine for managing stress-related disorders, optimizing performance in sports science, and monitoring physiological strain in occupational health settings.

References

1 B. Wang, C. Zhao, Z. Wang, K.-A. Yang, X. Cheng, W. Liu, W. Yu, S. Lin, Y. Zhao, K. M. Cheung, H. Lin, H. Hojaiji, P. S. Weiss, M. N. Stojanović, A. J. Tomiyama, A. M. Andrews, and S. Emaminejad: Sci. Adv. **8** (2022) eabk0967. https://doi.org/10.1126/sciadv.abk0967

2 E. Knezevic, K. Nenic, V. Milanovic, and N. N. Knezevic: Cells **12** (2023) 2726. https://doi.org/10.3390/cells12232726

3 N. P. Bowles, S. S. Thosar, M. P. Butler, N. A. Clemons, L. D. Robinson, O. H. Ordaz, M. X. Herzig, A. W. McHill, S. P. M. Rice, J. Emens, and S. A. Shea: Front. Neurosci. **16** (2022) 995452. https://doi.org/10.3389/fnins.2022.995452

4 A. F. Turcu, L. Zhao, X. Chen, R. Yang, J. Rege, W. E. Rainey, J. D. Veldhuis, and R. J. Auchus: Eur. J. Endocrinol. **185** (2021) K1. https://doi.org/10.1530/EJE-21-0348

5 K. Tervahartiala, L. Perasto, S. Kortesluoma, R. Korja, H. Karlsson, S. Nolvi, and L. Karlsson: Psychoneuroendocrinology **156** (2023) 106345. https://doi.org/10.1016/j.psyneuen.2023.106345

6 Z. Zajkowska, N. Gullett, A. Walsh, V. Zonca, G. A. Pedersen, L. Souza, C. Kieling, H. L. Fisher, B. A. Kohrt, and V. Mondelli: Psychoneuroendocrinology **136** (2022) 105625. https://doi.org/10.1016/j.psyneuen.2021.105625

7 C. Mennitti, G. Farina, A. Imperatore, G. De Fonzo, A. Gentile, E. La Civita, G. Carbone, R. R. De Simone, M. R. Di Iorio, N. Tinto, G. Frisso, V. D'Argenio, B. Lombardo, D. Terracciano, C. Crescioli, and O. Scudiero: Biomolecules **14** (2024) 1418. https://doi.org/10.3390/biom14111418

8 A. Deeb, A. Babiker, S. Sedaghat, A. El Awwa, K. Gupta, A. B. Pulungan, U. Isa Umar, Z. Akanov, S. Kalra, D. Zangen, S. Al Adhami, M. Karipidou, and M. L. Marcovecchio: Pediatr. Diabetes **23** (2022) 1512. https://doi.org/10.1111/pedi.13447
9 M. Spindler, M. Palombo, H. Zhang, and C. M. Thiel: Sci. Rep. **13** (2023) 6866. https://doi.org/10.1038/s41598-023-33922-5
10 L. Wu, W. Xu, H. Li, B. Dong, H. Geng, J. Jin, D. Han, H. Liu, X. Zhu, Y. Yang, and S. Xie: Antioxidants **11** (2022) 935. https://doi.org/10.3390/antiox11050935
11 O. Karin, M. Raz, A. Tendler, A. Bar, Y. Korem Kohanim, T. Milo, and U. Alon: Mol. Syst. Biol. **16** (2020) e9510. https://doi.org/10.15252/msb.20209510
12 M. H. Bergkamp, S. Cajigas, L. J. van IJzendoorn, and M. W. J. Prins: ACS Sens. **8** (2023) 2271. https://doi.org/10.1021/acssensors.3c00245
13 S. Shin, H. Oh, H. R. Park, E. Y. Joo, and S.-Y. Lee: Ann. Lab. Med. **41** (2021) 108. https://doi.org/10.3343/alm.2021.41.1.108
14 C. Wang, Z. Wang, W. Wei, Z. Zhang, A. A. Li, G. Huang, X. Li, S. S. Ge, L. Zhou, and H. Kong: npj Flex. Electron. **8** (2024) 47. https://doi.org/10.1038/s41528-024-00333-z
15 P. Pearlmutter, G. DeRose, C. Samson, N. Linehan, Y. Cen, L. Begdache, D. Won, and A. Koh: Sci. Rep. **10** (2020) 19050. https://doi.org/10.1038/s41598-020-75871-3
16 S. Yeasmin, A. Ullah, B. Wu, X. Zhang, and L.-J. Cheng: ACS Appl. Mater. Interfaces **15** (2023) 50034. https://doi.org/10.1021/acsami.3c11374
17 P. Krishnaveni and V. Ganesh: Sci. Rep. **11** (2021) 7663. https://doi.org/10.1038/s41598-021-86866-z
18 K. Theyagarajan and Y.-J. Kim: Biosensors **13** (2023) 424. https://doi.org/10.3390/bios13040424
19 Y. Li, L. Luo, Y. Kong, Y. Li, Q. Wang, M. Wang, Y. Li, A. Davenport, and B. Li: Biosens. Bioelectron. **249** (2024) 116018. https://doi.org/10.1016/j.bios.2024.116018
20 V. Sharma, T. K. Sharma, and I. Kaur: J. Appl. Electrochem. **53** (2023) 1765. https://doi.org/10.1007/s10800-023-01881-4
21 Z. Wang, Y. Shao, Z. Zhu, J. Wang, X. Gao, J. Xie, Y. Wang, Q. Wu, Y. Shen, and Y. Ding: Coord. Chem. Rev. **495** (2023) 215369. https://doi.org/10.1016/j.ccr.2023.215369
22 X. Ren, D. Chen, Y. Wang, H. Li, Y. Zhang, H. Chen, X. Li, and M. Huo: J. Nanobiotechnol. **20** (2022) 92. https://doi.org/10.1186/s12951-022-01295-y
23 J. A. Martin, J. L. Chávez, Y. Chushak, R. R. Chapleau, J. Hagen, and N. Kelley-Loughnane: Anal. Bioanal. Chem. **406** (2014) 4637. https://doi.org/10.1007/s00216-014-7883-8
24 C. Niu, Y. Ding, C. Zhang, and J. Liu: Sens. Diagn. **1** (2022) 541. https://doi.org/10.1039/D2SD00042C
25 A. R. Prado, J. P. Oliveira, B. A. Milaneze, B. V. Nogueira, M. C. C. Guimarães, L. C. P. Almeida, A. F. Neto, M. J. Pontes, and M. R. N. Ribeiro: Proc. SPIE **9286** (2014) 92862J. https://doi.org/10.1117/12.2063775
26 N. K. Singh, S. Chung, M. Sveiven, and D. A. Hall: ACS Omega **6** (2021) 27888. https://doi.org/10.1021/acsomega.1c03552
27 G. G. Urizar, H. S. Hernandez, J. Rayo, and S. Bhansali: Neurobiol. Stress **13** (2020) 100263. https://doi.org/10.1016/j.ynstr.2020.100263
28 S. Ghosh, P. Singh, S. Roy, K. Bhardwaj, and A. Jaiswal: ChemBioChem **23** (2022) e202100691. https://doi.org/10.1002/cbic.202100691
29 E. B. E. Domany, T. M. Essam, A. E. Ahmed, and A. A. Farghali: J. Appl. Pharm. Sci. **8** (2018) 119. https://doi.org/10.7324/JAPS.2018.8516
30 S. Honary, E. Gharaei-Fathabad, Z. K. Paji, and M. Eslamifar: Trop. J. Pharm. Res. **11** (2012) 887. https://doi.org/10.4314/tjpr.v11i6.3
31 Y. Jiang, M. Shi, Y. Liu, S. Wan, C. Cui, L. Zhang, and W. Tan: Angew. Chem. Int. Ed. **56** (2017) 11916. https://doi.org/10.1002/anie.201703807
32 P. S. Kumar, K. G. Pavithra, and M. Naushad: Nanomaterials for Solar Cell Applications, S. Thomas, E. H. M. Sakho, N. Kalarikkal, S. O. Oluwafemi, and J. Wu, Eds. (Elsevier, 2019) p. 85. https://doi.org/10.1016/B978-0-12-813337-8.00004-7
33 P. P. Sarkar, A. Ashraf, A. H. Jalal, F. Alam, and N. Islam: Biosensors **15** (2025) 321. https://doi.org/10.3390/bios15050321
34 A. Singh, A. Kaushik, R. Kumar, M. Nair, and S. Bhansali: Appl. Biochem. Biotechnol. **174** (2014) 1115. https://doi.org/10.1007/s12010-014-0894-2
35 V. Vignesh, B. Castro-Dominguez, T. D. James, J. M. Gamble-Turner, S. Lightman, and N. M. Reis: ACS Sens. **9** (2024) 1666. https://doi.org/10.1021/acssensors.3c01912
36 S. Dalirirad, D. Han, and A. J. Steckl: ACS Omega **5** (2020) 32890. https://doi.org/10.1021/acsomega.0c03223
37 S. M. Mugo, W. Lu, and S. Robertson: Biosensors **12** (2022) 854. https://doi.org/10.3390/bios12100854

38 S. M. Mugo and J. Alberkant: Anal. Bioanal. Chem. **412** (2020) 1825. https://doi.org/10.1007/s00216-020-02430-0
39 J. Liu, N. Xu, H. Men, S. Li, Y. Lu, S. S. Low, X. Li, L. Zhu, C. Cheng, G. Xu, and Q. Liu: Sensors **20** (2020) 1422. https://doi.org/10.3390/s20051422
40 B. Yang, H. Li, C. Nong, X. Li, and S. Feng: Anal. Biochem. **669** (2023) 115117. https://doi.org/10.1016/j.ab.2023.115117
41 G. Karuppaiah, M.-H. Lee, S. Bhansali, and P. Manickam: Biosens. Bioelectron. **239** (2023) 115600. https://doi.org/10.1016/j.bios.2023.115600
42 S. N. Alvi, K. Abuhdeeb, and M. M. Hammami: Adv. Pharmacol. Pharm. Sci. **2022** (2022) 3133640. https://doi.org/10.1155/2022/3133640
43 J. Ok, S. Park, Y. H. Jung, and T. Kim: Adv. Mater. **36** (2024) 2211595. https://doi.org/10.1002/adma.202211595